Laser-assisted charge-transfer collisions: $K^+ + Na$

Y. P. Hsu, M. Kimura, and R. E. Olson
Department of Physics, University of Missouri—Rolla, Rolla, Missouri 65401
(Received 11 June 1984; revised manuscript received 24 September 1984)

A theory has been formulated to characterize charge-transfer collisions in the presence of an external laser field. The molecular-state-expansion method is used to describe the scattering process within the impact-parameter formalism. Electron translation factors are included in the molecular-state expansion so that the scattering wave function satisfies the correct boundary conditions. The theory is applied to the process $K^+ + Na \rightarrow K + Na^+$. In addition, we have made a detailed analysis of laser-assisted charge transfer for low-energy collisions. In this case, a Landau-Zener formula can be derived which shows that the cross section increases with decreasing incident energy. In general the laser coupling is dominant in the low-energy region, while the dynamical coupling becomes important as the collision energy increases.

I. INTRODUCTION

Ion-atom charge-transfer processes have important applications in the areas of laser physics and fusion research. These processes are well studied.[1,2] However, in the low-energy collision regime, the energy defect of the donor (atom) and the acceptor (ion) severely suppresses the charge-transfer cross section. There is interest in using a laser to overcome the energy defect factor and thereby obtain a large charge-transfer cross section.[3–6] With the exception of Ref. 6, most authors did not use accurate values for the molecular-state energies and coupling matrix elements when they were calculating the laser-assisted charge-transfer cross sections. We propose to do a detailed analysis of the laser-assisted charge-transfer collision of $K^+ + Na$ in this paper, and, unlike in previous works, we have included the collisional-induced coupling term in our calculation.

Our calculations indicate that the laser-assisted charge transfer is important mainly in the low-collision-velocity region where collision-induced transitions are negligible. At higher velocities, collision-induced processes dominate. In the small crossover region where both mechanisms are important, the charge-transfer cross section shows an interference effect between these two mechanisms. Another important feature of the laser-assisted charge-transfer collision is that except at very low-collision velocities, the charge-transfer transition takes place in a much wider region than just around the "resonance point." The reason for this is that although the laser beam has been directed at the collision region for a long while, the interaction between the laser and the active electron is switched off as soon as the charge-transfer participants depart from each other. The finiteness of the reaction time would diffuse the transition region. At very low velocity the transition does take place only around the resonance point. A Landau-Zener type of formula can then be derived which shows that a cross section increases as the collision velocity is decreased.

In Secs. II and III we derive the coupled equations needed to study the charge-transfer process of $K^+ + Na$ under the influence of a laser beam. An experimental set-up is suggested for concrete computation. The molecular-state-expansion method is used to describe the scattering processes within the impact-parameter formalism. Electron translation factors (ETF's) are incorporated in the expansion so that the scattering wave function satisfies the correct boundary conditions. The coupling between laser and electron is treated semiclassically. The dipole approximation is used throughout the paper.

In Sec. IV, the formulas presented in Secs. II and III are applied to the test case of $K^+ + Na$ charge-transfer collisions. Several of the approximations made in the previous sections are justified in this section. The internuclear-distance dependence of the laser coupling matrix element is explained and the cross sections for charge transfer are computed with and without the laser for various incident velocities. A comparison of these cross sections reveals the relative importance of laser-induced versus collisional-induced charge transfer at different collision velocities. We also have calculated the cross sections using different laser frequencies to probe the validity of "resonance condition." Finally, the coupled equations are integrated to check the validity of the Landau-Zener formula for the cross section at very low velocity.

II. THEORETICAL FORMULATION

In this section we will derive the coupled equations needed for the calculations of laser-assisted charge transfer in an ion-atom collision system.[7] The one-electron problem will be treated here. Generalization to many-electron systems should present no further conceptual problem. The specific example of $Na + K^+$ charge transfer will be used to illustrate the points discussed here.

The notation and coordinate system will be defined first. We will follow closely the convention and notation used by Delos.[1] Shown in Fig. 1 are electron position vectors relative to nucleus A, the center of mass of the nuclei (CMN) and nucleus B, respectively. In the (space-fixed) CMN frame, the relative nuclear velocity $\mathbf{V} = d\mathbf{R}/dt$ is as

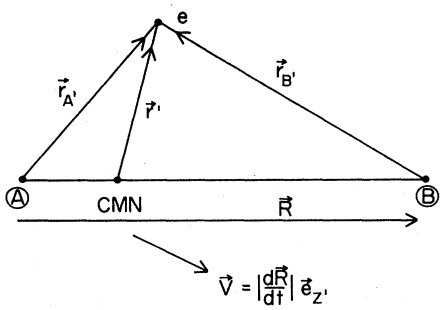

FIG. 1. Electron position relative to nucleus A, nucleus B, and center of mass of the nuclei (CMN) is represented by $\mathbf{r}'_A$, $\mathbf{r}'_B$, and $\mathbf{r}'$ vectors, respectively. The internuclear distance is represented by $\mathbf{R}$. $\mathbf{V}$ is the relative velocity. In this space-fixed CMN frame all position vectors are superscripted by a prime.

usual defined to be in the Z direction. We will also need the (rotating) molecular frame because the Born-Oppenheimer electronic states are usually solved in this coordinate frame. Following this convention, the internuclear axis $\mathbf{R}$ is defined as the Z axis in the molecular frame (see Fig. 2). If the angle between $\mathbf{R}$ and $\mathbf{V}$ is θ, then the electronic coordinates in the CMN frame, $\mathbf{r}'=(x',y',z')$, and in the molecular frame, $\mathbf{r}=(x,y,z)$, are related by

$$\begin{aligned} x' &= x\cos\theta + z\sin\theta \ , \\ y' &= y \ , \end{aligned} \tag{1}$$

and

$$z' = -x\sin\theta + z\cos\theta \ .$$

An experimental setup we have in mind is depicted in Fig. 3. An atomic beam travels in the laboratory $\mathbf{z}$ direction and an ionic beam crosses it at a right angle, heading in the laboratory $\mathbf{x}$ direction. A laser beam is oriented in the laboratory $\mathbf{y}$ direction, such that the polarization points in the $\mathbf{z}$ direction in the CMN frame. There is no particular reason why the laser beam should be perpendicular to the collision plane or why the polarization should be parallel to the relative nuclear velocity. However, this

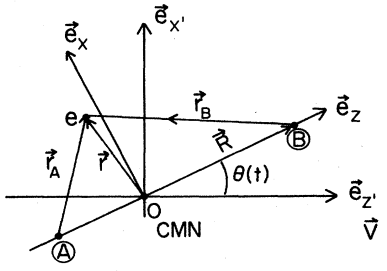

FIG. 2. (Rotating) molecular frame makes an angle of θ with respect to the (space-fixed) CMN frame. The two frames share a common reference point, the position of CMN. The electron position vector $\mathbf{r}$ in the molecular frame is related to the same vector in the CMN frame $\mathbf{r}'$ by formula (1).

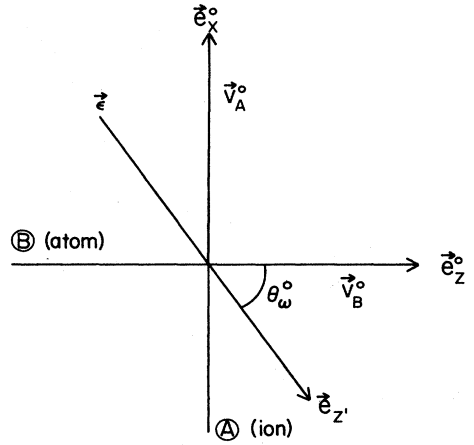

FIG. 3. Cross-beam experiment setup. The atomic and ionic beams which participate in the charge-transfer collision cross each other at right angle. A laser beam pointing in a direction perpendicular to the collision plane has been directed at the interaction region. If the polarization, ϵ, of the laser beam makes and angle $\theta^0_\omega = \cos^{-1}(v^0_B/v)$ with the atomic beam, the polarization will be in the $\mathbf{z}$ direction in the CMN frame. $\mathbf{V}^0_A$ and $\mathbf{V}^0_B$ are, respectively, the velocity vectors of the atomic and ionic beams in the laboratory frame, and $\mathbf{v}$ is the relative nuclear velocity vector.

setup does provide a concrete example when we discuss the theory and perform definite calculations.

Let us briefly review the theoretical formulation for the case when the laser beam is turned off. Assuming that the nuclear motion is described classically by $\mathbf{R}(t)$, we solve the resulting time-dependent Schrödinger equation for the electron. The state vector is expanded in an ETF-modified molecular-state basis,

$$\psi(r;t) = \sum_n a_n(t)\phi_n(\mathbf{r};\mathbf{R}(t)) \times \exp\left[\frac{im}{2\hbar}\mathbf{v}\cdot\mathbf{r} f_n(\mathbf{r};\mathbf{R})\right] , \tag{2}$$

where

$$f_n \rightarrow \left[\frac{M_A - M_B}{M_A + M_B}\right] \mp 1 \quad \text{as } R\rightarrow\infty \ , \tag{3}$$

and $\phi_n(\mathbf{r};\mathbf{R})$ is an atomic state centered on nucleus A (B) as $R\rightarrow\infty$. Note that the ϕ_n's are the usual Born-Oppenheimer states which satisfy

$$H_e(\mathbf{r};\mathbf{R})\phi_n(\mathbf{r};\mathbf{R}) = \epsilon_n(R)\phi_n(\mathbf{r};\mathbf{R}) \ . \tag{4}$$

Substituting (2) into the time-dependent Schrödinger equation, we obtain the following coupled equation which is correct up to first order in $\mathbf{V}$:[1]

$$i\hbar\dot{a}_i = \epsilon_i a_i + \mathbf{V}\cdot\sum_j (\mathbf{P}+\mathbf{A})_{ij} a_j + O(\mathbf{V}^2) \ , \tag{5}$$

where

$$p_{ij}=\langle\phi_i\,|\,(-i\hbar\nabla_{\mathbf{R}})\,|\,\phi_j\rangle\ , \tag{6}$$

and

$$A_{ij}=\left[\frac{im}{\hbar}\right]\langle\phi_i\,|\,[H_e,\tfrac{1}{2}f_j\mathbf{r}]\,|\,\phi_j\rangle\ . \tag{7}$$

When the laser beam is turned on, the Hamiltonian

$$H_e=\frac{1}{2m}P^2+V(r) \tag{8}$$

will change to

$$H_e^{\gamma}=\frac{1}{2m}\left[\mathbf{P}-\frac{e}{c}\mathbf{A}\right]^2+V(r)\ . \tag{9}$$

In the Coulomb gauge, $\nabla\cdot\mathbf{A}=0$, so that

$$H_e^{\gamma}=H_e+H'\ , \tag{10}$$

where

$$H'=-\frac{e}{mc}\mathbf{A}\cdot\mathbf{P}+\frac{e^2}{2mc}A^2\ . \tag{11}$$

If the power of the laser beam is not high, $|\,eA/c\,|\ll p$, we can drop the nonlinear term in (11), and approximate H' by

$$H'=-\frac{e}{mc}\mathbf{A}\cdot\mathbf{P}\ . \tag{12}$$

H' will be treated as a small perturbation compared to H_e of Eq. (8). The coupled equation (5), when the laser-interacting terms are included, becomes

$$i\hbar\dot{a}_i=\epsilon_i a_i+\mathbf{V}\cdot\sum_j(\mathbf{P}+\mathbf{A})_{ij}a_j+\sum_j\langle\phi_i\,|\,H'\,|\,\phi_j\rangle a_j+O(\mathbf{V}^2,\mathbf{A}^2,\mathbf{V}\cdot\mathbf{A})\ . \tag{13}$$

In Eq. (13) we have neglected terms of order $\mathbf{V}^2$, $\mathbf{A}^2$, $\mathbf{V}\cdot\mathbf{A}$, or higher.

Within the dipole approximation the laser coupling terms become

$$\langle\phi_i\,|\,H'\,|\,\phi_j\rangle=\left[-\frac{e}{mc}\right]2\,|\,A_0\,|\cos(\omega t)\boldsymbol{\epsilon}\cdot\langle\phi_i\,|\,\mathbf{P}\,|\,\phi_j\rangle$$

$$=\left[-\frac{ie}{\hbar c}\right](\epsilon_i-\epsilon_j)2\,|\,A_0\,|\cos(\omega t)\boldsymbol{\epsilon}\times\langle\phi_i\,|\,\mathbf{r}\,|\,\phi_j\rangle\ , \tag{14}$$

where $\boldsymbol{\epsilon}$ is the polarization vector. If we further assume that the polarization of the laser beam is pointing in the $\mathbf{z}$ direction in the CMN frame (see Fig. 3), then Eq. (14) becomes

$$\langle\phi_i\,|\,H'\,|\,\phi_j\rangle=\left[-\frac{ie}{\hbar c}\right](\epsilon_i-\epsilon_j)2\,|\,A_0\,|\cos(\omega t)\langle\phi_j\,|\,z'\,|\,\phi_j\rangle$$

$$=\left[\frac{ie}{\hbar}\right]\frac{(\epsilon_i-\epsilon_j)}{\omega}\left[-\frac{\omega 2\,|\,A_0\,|}{c}\cos(\omega t)\right](-\langle\phi_i\,|\,x\,|\,\phi_j\rangle\sin\theta+\langle\phi_i\,|\,z\,|\,\phi_j\rangle\cos\theta)\ . \tag{15}$$

In the last step, we have used the relationship given in (1). By using a linear trajectory of the form

$$R(t)=\mathbf{b}+\mathbf{v}t \tag{16}$$

(see Fig. 4), we finally have the following form for the laser coupling terms:

$$\langle\phi_i\,|\,H'\,|\,\phi_j\rangle=\left[\frac{-i\,|\,e\,|}{\hbar}\right]\frac{(\epsilon_i-\epsilon_j)}{\omega}\left[\frac{2\omega\,|\,A_0\,|}{c}\cos(\omega t)\right]\left[\langle\phi_i\,|\,x\,|\,\phi_j\rangle\frac{b}{\sqrt{b^2+v^2t^2}}-\langle\phi_i\,|\,z\,|\,\phi_j\rangle\frac{vt}{\sqrt{b^2+v^2t^2}}\right]\ . \tag{17}$$

Formulas (13), (6), (7), and (17) are the basis for our numerical calculations. In the spherical coordinate system where $\mathbf{R}=(R,\theta,\phi=0)$, we can decompose the matrix elements of (6) and (7) into their "radial" and "angular" parts:

$$P_{ij}=\langle\phi_i\,|\,P\,|\,\phi_j\rangle=\mathbf{e}_R P_{ij}^R+\mathbf{e}_\theta P_{ij}^\theta \tag{18}$$

and

$$A_{ij}=\langle\phi_i\,|\,A\,|\,\phi_j\rangle=\mathbf{e}_R A_{ij}^R+\mathbf{e}_\theta A_{ij}^\theta\ , \tag{19}$$

where

$$P_{ij}^R=\left\langle\phi_i\,\middle|\,\left[-i\hbar\frac{\partial}{\partial R}\right]\,\middle|\,\phi_j\right\rangle\ , \tag{20}$$

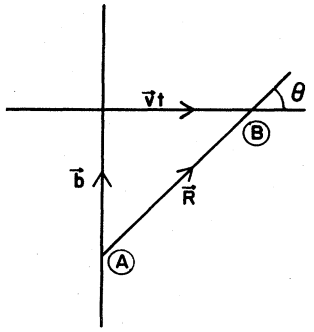

FIG. 4. A linear trajectory is used to describe the relative nuclear motion. $\mathbf{b}$ is the impact parameter vector, which is perpendicular to the relative velocity vector $\mathbf{v}$. The angle between $\mathbf{R}$, the internuclear distance vector, and $\mathbf{v}$ is $\theta(t)$.

$$P_{ij}^{\theta} = -R^{-1}\langle \phi_i \mid L_y \mid \phi_j \rangle \ , \tag{21}$$

$$A_{ij}^{R} = \left[\frac{im}{\hbar}\right]\langle \phi_i \mid [H_e, \tfrac{1}{2} f_j z] \mid \phi_j \rangle \ , \tag{22}$$

and

$$A_{ij}^{\theta} = \left[\frac{im}{\hbar}\right]\langle \phi_i \mid [H_e, \tfrac{1}{2} f_j x] \mid \phi_j \rangle \ . \tag{23}$$

III. EXAMPLE

In the following we will apply the above formulas to the charge transfer collision of

$$K^+ + Na(3s) + \gamma \rightarrow K(4s) + Na^+ \ . \tag{24}$$

The frequency of the laser beam will be chosen to be in resonance with the energy difference between the $1^2\Sigma$ and $2^2\Sigma$ molecular states of the NaK^+ system. The $1^2\Sigma$ state is asymptotically connected to the atomic $Na(3s)$ state while the $2^2\Sigma$ state is asymptotically connected to the atomic $K(4s)$ state. For simplicity we will only consider the coupling between the $1^2\Sigma$ and $2^2\Sigma$ states. The inclusion of more molecular states does not change the physics, especially at low-collision velocities.

For Σ-Σ coupling, the angular matrix element of (21) is zero. Similarly, because the transition dipole moment, when sandwiched between two Σ states, does not have either x or y components, Eq. (23) is also equal to zero. Therefore, in (18) and (19) only the radial coupling terms survive. It is then necessary to solve the following coupled equations:

$$i\hbar \dot{a}_1 = \epsilon_1 a_1 + v^R (P_{12}^R + A_{12}^R) a_2 + i f a_2 \ , \tag{25}$$

and

$$i\hbar \dot{a}_2 = \epsilon_2 a_2 + v^R (P_{12}^R + A_{12}^R) a_1 - i f a_1 \ , \tag{26}$$

where

$$f = -\frac{|e|}{\hbar}\frac{(\epsilon_2 - \epsilon_1)}{\omega}\left[\frac{|A_0|\omega}{c}\right](e^{i\omega t} + e^{-i\omega t}) \times \frac{vt}{\sqrt{b^2 + v^2 t^2}}\langle \phi_1 \mid z \mid \phi_2 \rangle \ . \tag{27}$$

Let us now discuss the low-velocity behavior of the coupled equations, (25) and (26). In the limit of low-collision velocity, the dynamical couplings are not important and they may be safely neglected. We have then

$$i\hbar \dot{a}_1 \simeq \epsilon_1 a_1 + i f a_2 \tag{28}$$

and

$$i\hbar \dot{a}_2 \simeq \epsilon_2 a_2 - i f a_1 \ . \tag{29}$$

The equations can be rewritten as

$$\dot{\tilde{a}}_1 = \frac{1}{\hbar}\left[f \exp\left[-\frac{i}{\hbar}\int_0^t (\epsilon_2 - \epsilon_1) dt'\right]\right]\tilde{a}_2 \tag{30}$$

and

$$\dot{\tilde{a}}_2 = \frac{-1}{\hbar}\left[f \exp\left[\frac{i}{\hbar}\int_0^t (\epsilon_2 - \epsilon_1) dt'\right]\right]\tilde{a}_1 \ , \tag{31}$$

where

$$a_i = \tilde{a}_i \exp\left[-\frac{i}{\hbar}\int_0^t \epsilon_i \, dt'\right] \ . \tag{32}$$

At low-collision velocity, the rotational wave approximation (RWA) can be used. The factors inside the outer parentheses in (30) and (31) can then be simplified to

$$f \exp\left[\mp \frac{i}{\hbar}\int_0^t (\epsilon_2 - \epsilon_1) dt'\right] = f_0 \exp\left[\mp \frac{i}{\hbar v}\alpha\right] \ , \tag{33}$$

where

$$f_0 = -\frac{|e|}{\hbar}\frac{(\epsilon_2 - \epsilon_1)}{\omega}\left[\frac{|A_0|\omega}{c}\right] \times \langle \phi_1 \mid z \mid \phi_2 \rangle \frac{vt}{\sqrt{b^2 + v^2 t^2}} \tag{34}$$

and

$$\alpha = \int_b^{R(t)} (\epsilon_2 - \epsilon_1 - \hbar\omega)\frac{R dR}{\sqrt{R^2 - b^2}} \ . \tag{35}$$

The coupled equations of (30) and (31) in the RWA approximation now become

$$i\hbar \frac{d\tilde{a}_1}{dR} = +i\left[\frac{\Delta_0}{v}\right]\exp\left[-\frac{i}{\hbar v}\alpha\right]\tilde{a}_2 \tag{36}$$

and

$$i\hbar \frac{d\tilde{a}_2}{dR} = -i\left[\frac{\Delta_0}{v}\right]\exp\left[\frac{i}{\hbar v}\alpha\right]\tilde{a}_1 \ , \tag{37}$$

where

$$\Delta_0 = \frac{-|e|}{\hbar}\frac{(\epsilon_2 - \epsilon_1)}{\omega}\left[\frac{|A_0|\omega}{c}\right]\langle \phi_1 \mid z \mid \phi_2 \rangle \ . \tag{38}$$

In this derivation we have used the fact that

$$\frac{d}{dt} = v\sqrt{1 - (b/R)^2}\frac{d}{dR} \ ,$$

when $t > 0$, and

$$\frac{d}{dt} = -v\sqrt{1 - (b/R)^2}\frac{d}{dR} \ ,$$

when $t < 0$.

It is apparent that when v increases, (Δ_0/v) becomes small, and the laser coupling term is not as important as the dynamical coupling term. In fact both coupling terms operate in different velocity regions. For higher velocities the dynamical coupling term dominates, while at low velocities the laser coupling term dominates.

A Landau-Zener formula can be derived from the cou-

pled equations (36) and (37) at specified limits. If the relative velocity is low but still large enough such that $\Delta_0/v \ll 1$ a.u., then the first-order perturbation theory can be applied. This condition can be satisfied even at very low velocities, either because the transition dipole moment is small or because the intensity of laser beam is not large. Using the first-order perturbation theory, we have

$$\begin{aligned} |a_2(b;t\to\infty)|^2 &= |\tilde{a}_2(b;t\to\infty)|^2 \\ &= \left|\tilde{a}_2(b;t\to-\infty)-\frac{1}{\hbar}\int_{-\infty}^{\infty}dt' f_0(b;t')\exp\left[\frac{i}{\hbar v}\alpha(b;t')\right]\tilde{a}_1(b;t\to-\infty)\right|^2 \\ &= \left|\frac{1}{\hbar}\int_{-\infty}^{\infty}dt' f_0\exp\left[\frac{i}{\hbar v}\alpha\right]\right|^2 . \end{aligned} \tag{39}$$

In the last step we have used the fact that $|\tilde{a}_1(b,t\to-\infty)|=1$ and $|\tilde{a}_2(b,t\to-\infty)|=0$.

Let us compute the $t>0$ part of the integral first. In terms of the R integration, the integral is

$$\frac{1}{\hbar}\int_0^{\infty}dt' f_0\exp\left[\frac{i}{\hbar v}\alpha\right]=\int_0^{\infty}\left[\frac{\Delta_0}{\hbar v}\right]\exp\left[\frac{i}{\hbar v}\alpha(b;R)\right]dR . \tag{40}$$

However, since v is small, the contribution to the integral comes only from the neighborhood of $R=R_c$, where

$$\left.\frac{d\alpha(R)}{dR}\right|_{R=R_c}=0 . \tag{41}$$

This condition, Eq. (41), implies that R_c is the "resonance" point where

$$\epsilon_2(R_c)-\epsilon_1(R_c)=\hbar\omega . \tag{42}$$

Application of the stationary phase method is now in order. We have

$$\begin{aligned} \int_0^{\infty}\left[\frac{\Delta_0}{\hbar v}\right]\exp\left[\frac{i}{\hbar v}\alpha(R)\right]dR \simeq -\frac{|e|}{\hbar v}\left[\frac{|A_0|c}{c}\right]\exp\left[\frac{i}{\hbar v}\alpha(R_c)+\frac{i\pi}{4}\right] \\ \times\frac{2\pi\hbar v}{\left[\left|\dfrac{d^2\alpha(R)}{dR^2}\right|_{R=R_c}\right]^{1/2}}\langle\phi_1|z|\phi_2\rangle|_{R=R_c} , \end{aligned} \tag{43}$$

and therefore

$$|a_2(b;t\to\infty)|^2=2\frac{e^2}{\hbar^2v^2}\left[\frac{|A_0|\omega}{c}\right]^2\frac{2\pi\hbar v}{\left|\dfrac{d}{dR}(\epsilon_2-\epsilon_1)\right|_{R=R_c}}\left[1-\left[\frac{b^2}{R_c}\right]\right]^{1/2}|\langle\phi_1|z|\phi_2\rangle|^2_{R=R_c} . \tag{44}$$

In formula (44) we have incoherently added the two equal contributions from the $t>0$ and the $t<0$ integrals. Since v is small, the interference between these two contributions oscillates very rapidly with respect to b. When we integrate out $|a_2(b:t\to\infty)|^2$, with respect to b, the interference term just drops out. So we have

$$\begin{aligned} \sigma &= \int_0^{\infty}db\,2\pi b\,|a_2(b;t\to\infty)|^2 \\ &= \int_0^{R_c}db\,2\pi b\,|a_2|^2 \\ &= \frac{8\pi^2e^2R_c^2}{3\hbar v}\left[\frac{|A_0|^2\omega^2}{c^2}\right]\frac{|\langle\phi_1|z|\phi_2\rangle|^2_{R=R_c}}{\left|\dfrac{d}{dR}(\epsilon_2-\epsilon_1)\right|_{R=R_c}} . \end{aligned} \tag{45}$$

This formula is valid only for very low velocity where the stationary phase approximation is valid. Note that R_c is the resonance point where

$$\epsilon_2(R_c)=\epsilon_1(R_c)+\hbar\omega . \tag{46}$$

Formula (45) tells us that the cross section is inversely proportional to the collision velocity. It is the same as formula (13) of Errea *et al.*[6] except that instead of using

$$\left|\frac{d}{dR}(\epsilon_2-\epsilon_1)\right|_{R=R_c}$$

in the denominator, they have used

$$\left|\frac{d}{dt}(\epsilon_2-\epsilon_1)\right|_{t_0} ,$$

which can be shown to be dimensionally incorrect.

At higher velocities, the dipole coupling term becomes

smaller, as can be seen from Eqs. (36) and (37). The physics thereafter is the usual charge-transfer physics without the assistance of the laser field.

IV. NUMERICAL CALCULATIONS AND DISCUSSION

In this section we will study the laser-assisted charge-transfer process of (24). The coupled equations we need to solve are (25) and (26), which are appropriate for a two-state approximation. In order to prepare the coupling matrix elements needed in the equations, we have used the Born-Oppenheimer (BO) molecular states of $(NaK)^+$.

To obtain the BO molecular states, we have solved the following one-electron Schrödinger equation:

$$\left[-\tfrac{1}{2}\nabla_r^2+V_K(\mathbf{r}_A)+V_{Na}(\mathbf{r}_B)+\frac{1}{R}\right]\phi_n(\mathbf{r};R)=\epsilon_n\phi_n(\mathbf{r};R)\ , \tag{47}$$

where $\mathbf{r}_A$ and $\mathbf{r}_B$ are the position vectors of the valence electron relative to the K^+ and Na^+ ion cores, respectively. The potential $V_K(\mathbf{r}_A)$, which represents the interaction between the valence electron and potassium's ion core, is replaced by the pseudopotential.[8] The pseudopotentials we used for both the sodium and potassium ion cores are an l-dependent Gaussian type of the form

$$V_K(\mathbf{r})=\sum_{l,m}V_l(r)\,|\,Y_{lm}\rangle\langle\,Y_{lm}\,| \tag{48}$$

with

$$V_l(r)=A_l\exp(-\xi_l r^2)-\frac{\alpha_d}{2(r^2+d^2)^2}-\frac{\alpha_q}{2(r^2+d^2)^3}\ ,$$

where $|\,Y_{lm}\rangle$ are the spherical harmonics. The parameters A_l, ξ_l, α_d, α_q, and d are chosen to fit spectroscopic data and have been tabulated by Bardsley.[8]

The BO wave function $\phi_n(\mathbf{r};R)$ is constructed using a two-centered expansion in terms of a linear combination of atomic orbitals—molecular orbitals (LCAO-MO) method. Fixed orbital exponents in a Slater-type-orbital (STO) basis are used with the BO wave function given by

$$\phi_n(\mathbf{r};R)=\sum_i c_{in}X_i^{\mathrm{STO}}(\mathbf{r}_A)+\sum_j d_{jn}X_j^{\mathrm{STO}}(\mathbf{r}_B)\ . \tag{49}$$

For the $^2\Sigma^+$ molecular states, 18 STO's (nine on each center) have been employed. Each individual basis set includes p and d orbitals to account for polarization effects. The basis sets and the exponents used are tabulated in Table I. These orbital exponents are from Stevens *et al.*[9] and Kimura *et al.*[10] Note that in Table I, n represents the principle quantum number of the ground-state valence electron. The molecular potentials for the $1^2\Sigma$ and $2^2\Sigma$ states are shown in Fig. 5. Asymptotically the $2^2\Sigma$ state is connected to the potassium $4s$ atomic state, while the $1^2\Sigma$ state is connected to the sodium $3s$ atomic state. As can be seen from the graph, the two states do not change their isolated atomic characters until $R \lesssim 20$ a.u. and start to repel each other around $R=12$ a.u.

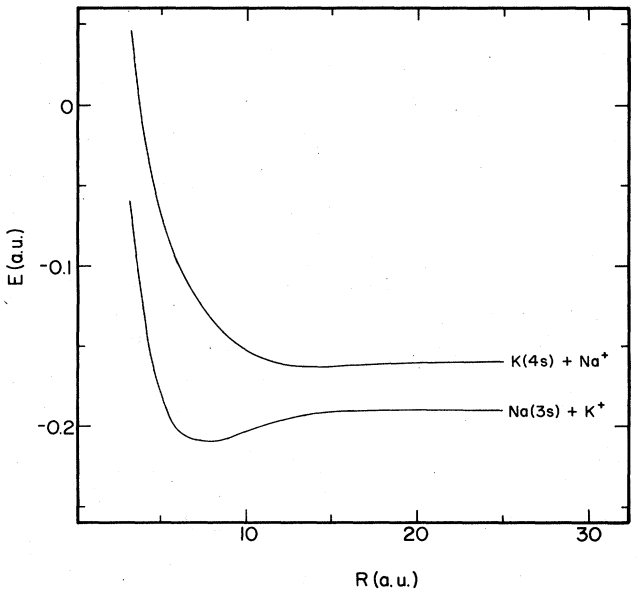

FIG. 5. Calculated potential energies for the $1^2\Sigma$ and $2^2\Sigma$ BO molecular states of $(NaK)^+$.

The radial coupling matrix elements, $\langle 1^2\Sigma\,|\,P^R+A^R\,|\,2^2\Sigma\rangle$ and $\langle 2^2\Sigma\,|\,P^R+A^R\,|\,1^2\Sigma\rangle$ are shown in Fig. 6. Note that in the calculation of radial matrix elements we have used the simple form of (3) for the switching functions, f_n, at all R. This type of atomic switching function is appropriate here since the radial matrix elements have maxima at $R\simeq 12$ a.u. The dynamical-coupling-induced transitions will take place at large internuclear separations.

Also shown in the graph is the z component (along the molecular axis) of the transition dipole moment $\langle 2^2\Sigma\,|\,z\,|\,1^2\Sigma\rangle$. As the graph indicates the transition dipole moment is small when $R>20$ a.u. and begins to increase as R decreases and reaches a maximum value of 3.25 a.u. at $R\approx 11$ a.u. After that it stays finite. Note that the R dependence of the transition dipole moment is similar to that of radial coupling matrix element, except that it is 20 times larger. The behavior of the transition dipole moment versus R can be explained as follows: At

TABLE I. Slater-orbital basis-set exponents.

	$(n-1)s$		ns		$(n+1)s$	np		$3d$	
Na	0.790	2.487	0.694	0.372	0.290	0.721	0.558	1.484	0.337
K	1.135	1.134	0.689	0.394	0.352	0.820	0.556	1.770	0.394

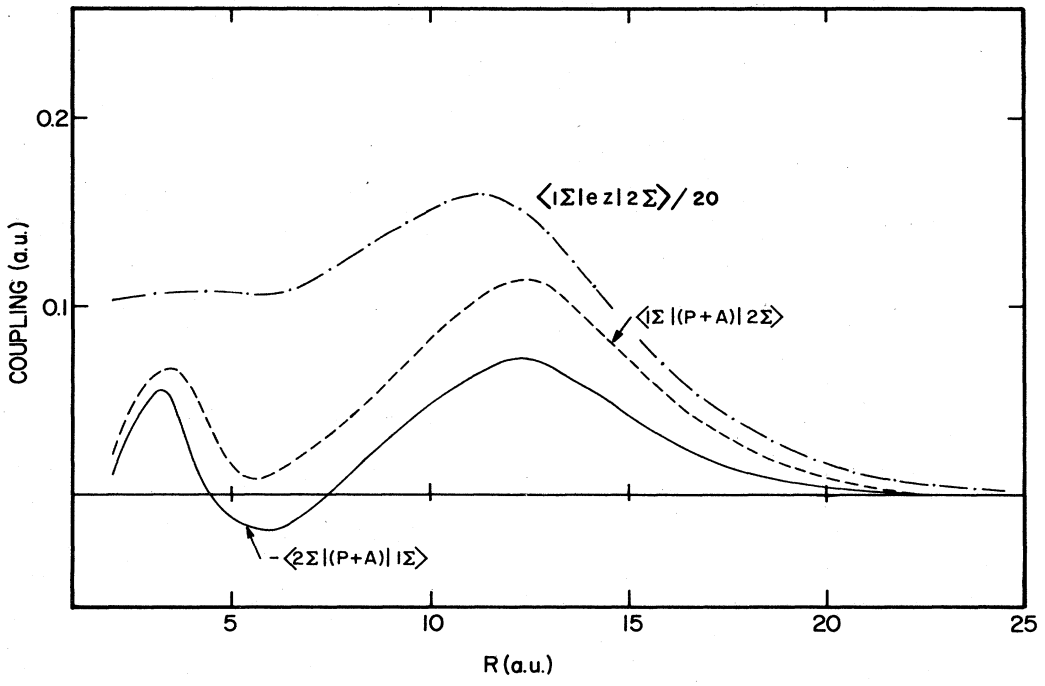

FIG. 6. Radial and laser coupling matrix elements computed between $1^2\Sigma$ and $2^2\Sigma$ states of $(NaK)^+$. The broken line is for the $\langle 1^2\Sigma \mid (p+A)_r \mid 2^2\Sigma \rangle$ radial matrix element and the solid line is for the $\langle 2^2\Sigma \mid (\mathbf{p}+\mathbf{A})_r \mid 1^2\Sigma \rangle$ radial matrix element. Both matrix elements peak around $R=12$ a.u. The dotted-dashed line represents the laser coupling matrix element of $\langle 2^2\Sigma \mid z \mid 1^2\Sigma \rangle = \langle 1^2\Sigma \mid z \mid 2^2\Sigma \rangle$, which peaks around $R=11$ a.u.

$R \gtrsim 20$ a.u., both $1^2\Sigma$ and $2^2\Sigma$ states are just atomic s states. Thus, an optical transition between these two states will not proceed since their transition matrix element is zero. As R decreases, polarization effects become important and the two Σ states begin to have some p- and d-wave components. A small nonzero transition dipole moment at these internuclear separations reflects this fact. As R decreases further, the overlap between the two Σ states increases, and at the same time they become more molecularlike. Both facts contribute to the increase in the transition dipole moment at small R. An examination of $1^2\Sigma$ and $2^2\Sigma$ molecular states at small R in Fig. 7 shows why the transition dipole moment is large. From Fig. 7 we see that $1^2\Sigma$ state wave function is of the same positive sign along the z (molecular axis) direction, while $2^2\Sigma$ state wave function is mostly negative for $z<0$ and positive for $z>0$. The product of the $1^2\Sigma$ and $2^2\Sigma$ wave functions therefore changes sign in phase with the z variable. The contribution from the $z<0$ part of the product wave function adds constructively to the $z>0$ part of the product wave function in computing the transition dipole moment. As R approaches zero we arrive at the united atom limit. The $1^2\Sigma$ and $2^2\Sigma$ states should approach Zn^+ $4s$ and $4p$ states, respectively. The transition dipole moment should therefore stay finite.

For our first set of calculations, we have used a laser power of 1 GW/cm^2. The following formula converts the power P in watts/cm^2 to the quantity $\omega \mid A_0/c$ in atomic units:

$$\frac{\omega \mid A_0 \mid}{c} = 2.6692 \times 10^{-9} \, [P(\text{watts/cm}^2)]^{1/2} . \quad (50)$$

We also choose an ω equal to the energy defect of Na $3s$ level and K $4s$ level. In atomic units $\omega = 0.029\,57$.[11] This is the resonance frequency for the $1^2\Sigma$ and $2^2\Sigma$ BO states

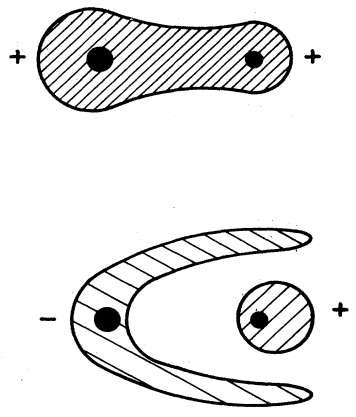

FIG. 7. A schematic plot of $1^2\Sigma$ and $2^2\Sigma$ state's wave functions in the "molecular" region. The upper one is for the $1^2\Sigma$ state while the lower one is for the $2^2\Sigma$ state. The Na^+ and K^+ cores are represented by two small black circles.

at $R \gtrsim 20$ a.u. But as mentioned in Sec. I, exact resonance is not important,[12] unless the collision velocity is very low. The results for the charge-transfer cross-section calculation is shown in Fig. 8. We have run the calculation for a range of velocities from 0.01 to 0.1 a.u. In order to see the relative importance of dynamical coupling versus laser coupling, we have also run the coupled equations (25) and (26) with each of the two coupling terms turned off. The results are plotted alongside the full calculations.

As a check on our calculations, we have computed the cross sections for the dynamical coupling case to $v=0.4$ a.u. and compare our results with the experimental data of Daley and Perel.[13] For $v \gtrsim 0.08$ a.u. their results agree well with ours, while at lower velocities their cross sections are much larger than ours. A look at their data for $Na^+ + Li$ and $K^+ + Na$ charge-transfer collisions show that the $K^+ + Na$ cross section decreases much more slowly near threshold than in the $Na^+ + Li$ case. This is contradictory to the fact that the energy defect of $K^+ + Na$ is larger than that of $Na^+ + Li$ and are therefore more vulnerable to a slowing down in collision velocity. Our calculations do agree with their $Na^+ + Li$ results down to $v=0.03$ a.u., which is the lower end of their data. We suggest that the experimental data on the $K^+ + Na$ charge-transfer cross sections at velocities below 0.08 a.u. are possibly too large.

From Fig. 8 one can see that the full calculation results start to deviate from the pure laser coupling results only when $v \gtrsim 0.03$ a.u., and for $v \gtrsim 0.07$ a.u. the results of the full calculation merge with the pure dynamical coupling calculation. This agrees with our discussion in Sec. II that laser coupling dominates the low-velocity region while the dynamical coupling dominates the high-velocity region. The two kinds of couplings are of equal importance only in the small region around $v \approx 0.05$ a.u., where the interference between these two couplings is evident.

It is interesting to examine the region where the effect of dynamical coupling is of the same magnitude as that of laser coupling. Shown in Fig. 9 is the graph of Pb versus b at $v=0.05$ a.u., where P is the charge-transfer transition probability at each impact parameter b. Note that the charge-transfer cross section is obtained by an integration over b of $2\pi Pb$. Three curves are plotted in Fig. 9, one for the case of the pure dynamical coupling case, another for the case of pure laser coupling, while the other is for the case of the combined couplings. The graph shows clearly the constructive interference effect between the dynamical coupling and the laser coupling in the impact-parameter region where charge transfer is significant.

In order to check the effect of different ω's on the charge-transfer cross section, we have performed another calculation using a $\omega=0.040\,61$ a.u., which is the resonance frequency at $R \simeq 11$ a.u. where the laser coupling matrix element is near its maximum (see Fig. 6). As can be seen from Fig. 10, even under this "optimum" condi-

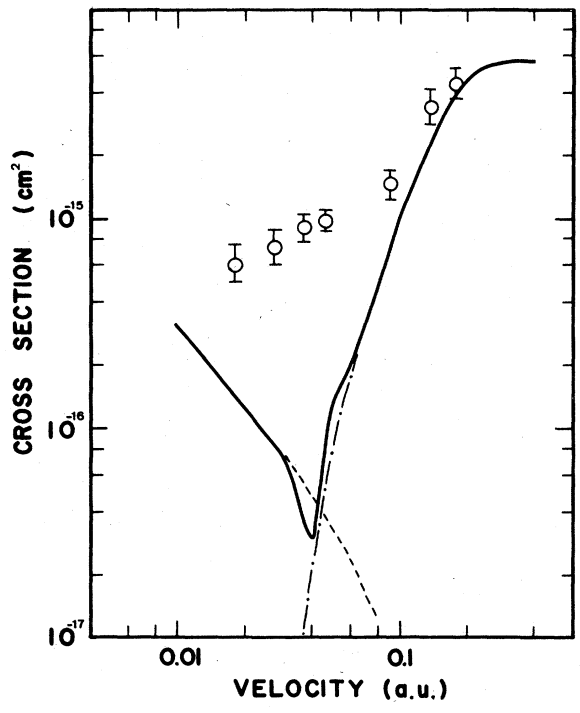

FIG. 8. Cross sections of the charge-transfer collision $K^+ + Na$ are plotted here. The solid line represents the result when both laser and collisional couplings are retained in the coupled equations. The dashed line represents the result when only laser coupling is considered, and the dotted-dashed line represents the charge-transfer cross section without the aid of the laser. The experimental charge-transfer result (without the employment of laser) of Daley and Perel is also plotted here, represented by the error bars.

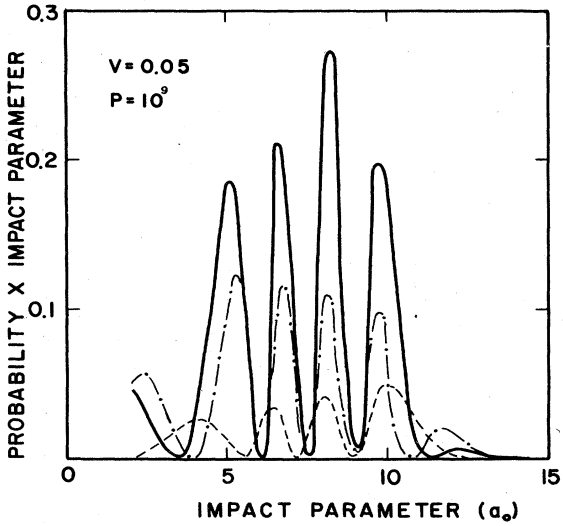

FIG. 9. $(p \times b)$ is plotted here versus the impact parameter b. Again the solid line represents the case when both laser coupling and collisional coupling are operating in the charge-transfer process. The dashed line represents the case when only laser coupling is operating, while the dotted-dashed line represents the charge-transfer collision with the laser coupling term turned off.

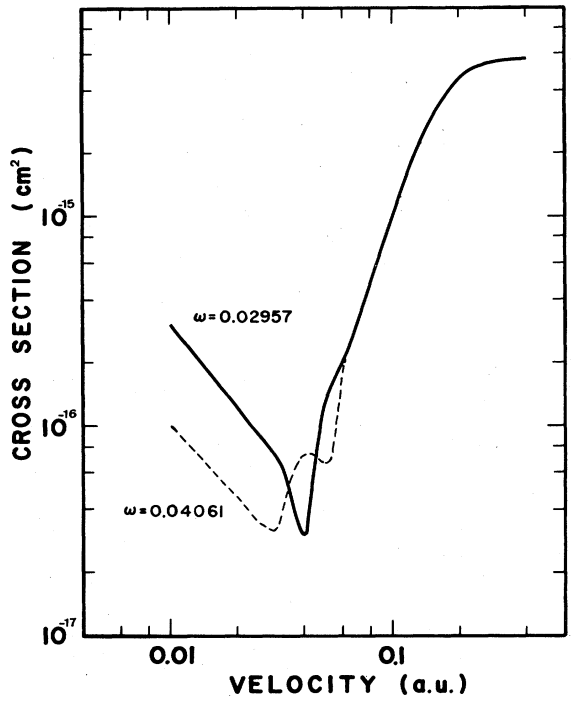

FIG. 10. Two charge-transfer cross sections using different laser frequencies are plotted here for various incident velocities. The dashed line is for $\omega=0.040\,61$ a.u. (11 220 Å) and the solid line is for $\omega=0.029\,57$ a.u. (15 409 Å).

tion for radiative transitions, the calculated cross section is no more than a factor of 3 different from the cross section we obtained early using a $\omega=0.029\,57$ a.u. in the velocity range from 0.01 to 0.1 a.u. In fact it is smaller. Note that the latter ω value is the resonance frequency for $R\gtrsim 20$ a.u. where the laser coupling matrix element is several orders of magnitude smaller than that at $R\approx 11$ a.u. Such results argue that the laser-induced charge-transfer transitions occur in a more diffuse region than just around the resonance points[14] if the collision velocity is not low. Like the case for $\omega=0.029\,57$ the cross section for $\omega=0.040\,61$ also shows the interference effect in the small region around $v\simeq 0.05$ a.u.

In the very low velocity region, $v<0.01$ a.u., it is necessary to observe the resonance condition just as in the case of isolated atomic system. Our Landau-Zener formula (45), which is based on the fact that transition takes place only in the neighborhood of the resonance points, then is applicable. Using a laser power of 1 GW/cm^2 and an ω value of 0.049 27 a.u., which corresponds to a resonance point at $R_c=10$ a.u., we can estimate the charge-transfer cross sections for various incident velocities. At $R=10$ a.u., $\langle\phi_1|z|\phi_2\rangle\approx 3.111\,65$ a.u. and $(d/dR)(\epsilon_2-\epsilon_1)=0.010\,07$. So we have

$$\sigma\approx\frac{0.018\,029}{v}\ \text{a.u.} \tag{51}$$

Formula (51) predicts a cross section of 1.2623×10^{-16} cm^2 at $v=0.004$ a.u. and a cross section of $0.841\,51\times10^{-16}$ cm^2 at $v=0.006$ a.u. Our calculated results at these velocities, obtained by solving the coupled equations (25) and (26), are, respectively, 1.4834×10^{-16} cm^2 and 0.9309×10^{-16} cm^2.[15] Indeed at very low velocities, the radiative transitions take place only in the neighborhood of the resonance points and the cross section is inversely proportional to the collision velocity as indicated by the Landau-Zener formula (45).

ACKNOWLEDGMENTS

The authors would like to thank Dr. B. R. Junker for providing us with the molecular-structure code. This research was supported by Physics Division, the U.S. Office of Naval Research.

[1]J. B. Delos, Rev. Mod. Phys. **53**, 287 (81).
[2]P. T. Greenland, Phys. Rep. **81**, 131 (82).
[3]R. Z. Vitlina, A. V. Chaplik, and M. V. Entin, Zh. Eksp. Teor. Fiz. **67**, 1667 (1974) [Sov. Phys.—JETP **40**, 829 (75)].
[4]D. A. Copeland and C. L. Tang, J. Chem. Phys. **65**, 3161 (76).
[5]M. H. Mittleman, Phys. Rev. A **14**, 586 (76).
[6]L. F. Errea, L. Mendez, and A. Riera, J. Chem. Phys. **79**, 4221 (83).
[7]For an early reference, see N. M. Kroll and K. M. Watson, Phys. Rev. A **13**, 1018 (1976).
[8]The pseudopotential methods are reviewed by J. N. Bardsley, Case Stud. At. Phys. **4**, 299 (1974).
[9]W. J. Stevens, A. M. Karo, and J. R. Hiskes, J. Chem. Phys. **74**, 3989 (1981).
[10]M. Kimura, R. E. Olson, and J. Pascale, Phys. Rev. A **26**, 3113 (1982).
[11]With these operational parameters, $\lambda=29118$ a.u. and $(e/c)|A_0|/P_e\approx(e/c)|A_0|=0.0903\ll 1$. Our use of the dipole approximation and the neglect of the nonlinear term in (12) is therefore justified.
[12]See also the latter part of Sec. IV and Ref. 6, especially Fig. 3.
[13]H. L. Daley and J. Perel, in *Proceedings of the Sixth International Conference on the Physics of Electronic and Atomic Collisions, Cambridge, Mass., 1969,* edited by I. Amdur (MIT, Cambridge, Mass., 1969).
[14]For not too small collision velocity, the interaction time for the laser and the atomic system is short. The uncertainty principle allows a wider transition region.
[15]The disagreement between the predicted and the calculated numbers can be attributed to the difficulty in estimating the energy derivative numerically.